PCCP

PAPER

View Article Online
View Journal | View Issue

Cite this: *Phys. Chem. Chem. Phys.*, 2017, **19**, 5839

Predicting bond dissociation energy and bond length for bimetallic diatomic molecules: a challenge for electronic structure theory†

Junwei Lucas Bao,[b] Xin Zhang,*[ab] Xuefei Xu[c] and Donald G. Truhlar*[b]

Received 30th December 2016,
Accepted 30th January 2017

DOI: 10.1039/c6cp08896a

rsc.li/pccp

Accurately predicting bond length and bond dissociation energy for bimetallic diatomic molecules that involve metal–metal multiple bonds is a great challenge for electronic structure theory, in part because many of these molecules have inherently multi-configuration wave functions, a characteristic that is variously labeled as strong correlation or multireference character. Although various popular density functionals are widely used in studying metal–metal bonding in catalysis, their accuracy can be questioned, and it is important to see both how well and how poorly a functional can perform. Here we test 50 Kohn–Sham exchange–correlation density functionals for selected 3d and 4d hetero- and homonuclear bimetallic diatomic molecules against experimental bond lengths and bond energies. We found that for the majority of the density functionals, the mean unsigned error in predicting the bond length is larger than 0.08 Å, and for the bond energy, half of the functionals give a mean unsigned error larger than 20 kcal mol^{-1}. This indicates that such highly multireference bimetallic systems are challenging for KS-DFT. However, some exchange–correlation functionals perform significantly better than average for both bond energies and bond lengths, in particular, BLYP, M06-L, N12-SX, OreLYP, RPBE, and revPBE, and are recommended for both kinds of calculations. Other functionals that perform relatively well for bond lengths include MGGA_MS0, MOHLYP, OLYP, PBE, and SOGGA11, and other functionals that perform relatively well for bond energies include GAM, M05, M06, MN15, and τ-HCTHhyb. Although some of these functionals (M05, M06, MN15, N12-SX, and τ-HCTHhyb) contain a nonzero percentage of Hartree–Fock exchange, a broader conclusion is that Hartree–Fock exchange brings in a static correlation error and usually tends to make the results, especially the bond lengths, less accurate. We find some significant differences between all-electron calculations and calculations with effective core potentials. For analysis, the article also presents CASSCF calculations of the percentage contributions of the dominant configurations, and the paper compares orbitals and configurations obtained in DFT calculations to those in CASSCF calculations. The equilibrium bond distance of Rh_2 is not available from experiments, and we predict it to be 2.22 Å. The bond energy of VCr is not available from experiments, and we predict it to be 52.9 kcal mol^{-1}.

1. Introduction

Being able to predict the structure and energy of metal–metal bonds is of fundamental importance for understanding and designing organometallic and inorganometallic catalysts,[1,2] but accurately describing metal–metal multiple bonds is not a simple task for electronic structure theory. Open-shell systems containing metal atoms are notoriously strongly correlated and coupled cluster calculations with affordable reference functions and affordable levels of excitation are not uniformly accurate for such systems, so almost all calculations on metal-containing systems for practical applications are carried out by Kohn–Sham density functional theory[3] (KS-DFT). Although validation studies have shown that modern exchange–correlation (XC) functionals can give good accuracy for most main group nonmetal chemistry,[4] it is harder to test the theory systematically for systems containing metal–metal bonds because of the scarcity of good data for bond lengths and bond energies of such systems. Bimetallic systems with partially filled d orbitals and multiple low-lying electronic configurations are inherently multi-configurational,

[a] *State Key Laboratory of Chemical Resource Engineering, Institute of Materia Medica, College of Science, Beijing University of Chemical Technology, Beijing, 100029, P. R. China. E-mail: zhangxin@mail.buct.edu.cn*
[b] *Department of Chemistry, Chemical Theory Center, and Supercomputing Institute, University of Minnesota, Minneapolis, Minnesota 55455-0431, USA. E-mail: truhlar@umn.edu*
[c] *Center for Combustion Energy, Tsinghua University, Beijing 100084, China*
† Electronic supplementary information (ESI) available. See DOI: 10.1039/c6cp08896a

and such systems (called multireference systems because a wave function calculation will converge well with respect to excitation level only if one uses a multi-configurational reference function) provide a severe test of KS-DFT, which uses a single Slater determinant (single electronic configuration) as a reference wave function.

The present work considers bimetallic diatomic molecules for which accurate experimental data are available. Several previous theoretical studies focus on 3d homonuclear diatomic bimetallic molecules;[5–9] and one recent interesting theoretical study explores the bonding pattern in superheavy transition-metal diatomics.[10] In our own previous work we studied atomic excitation energies in 3d transition metals[11] and 4d transion metals.[12] In this work, we consider selected 3d and 4d hetero- and homonuclear diatomics and systematically test 50 XC functionals against the most definitive experimental data available. The tests involve four 3d transition metals (Sc, V, Cr, and Co) and four 4d transition metals (Y, Nb, Mo, and Rh).

Coupled cluster theory[13–16] in the CCSD(T)[17] approximation is widely used as a benchmark for all kinds of chemistries, including transition-metal chemistry[18] (although many studies only involve metal–ligand rather than metal–metal bonds). However, recent studies have shown that CCSD(T) is not necessarily more accurate than some of the available XC functionals for predicting physical properties, such as the bond energy[19] and singlet–triplet gap,[20] of multireference systems. Furthermore, the cost of CCSD(T) is often prohibitive for large open-shell systems. The present paper is limited to KS-DFT, for which there is great interest in validation because calculations are affordable for large and complex systems.

Relativistic effects play an important role in the energetics of transition metals, especially for the 4d series and beyond. To account for scalar relativistic effects, one can use either a valence basis set combined with an effective core potential (ECP) or an all-electron basis set with a scalar relativistic Hamiltonian. The comparison of these methods is particularly interesting because the available ECPs were developed for wave function theory, but using them with density functional theory leads to additional uncertainties due to the nonlinear dependence of XC functionals on density, which leads to nonlinear core corrections.[21–26] To include vector relativistic effects, spin–orbit (SO) coupling would have to be calculated, although such calculations can be unaffordable for large systems and sometimes may be neglected for semi-quantitative work. For the purpose of the current benchmark, though, we did include such SO coupling contributions in the bond dissociation energies.

We emphasize that despite the difficulties for KS-DFT in describing intrinsically multireference transition metal–transition metal bonds, it is still being widely used for studying systems with metal–metal bonds, and the question of the accuracies of the various available exchange–correlation functionals is a recurring one. Therefore, it is critical to know not only how well the current approximate density functionals can perform, but also, and perhaps even more importantly, how poorly they sometimes perform. The latter can inform practitioners to what extent they can trust their calculations and can warn them to interpret their computational predictions with caution. Therefore, the present exhaustive test for bond energies and bond lengths for transition metal diatomics, which are the fundamental building blocks for large bimetallic complexes, is of essential value.

2. Experimental data

In the current work, our bimetallic diatomics dataset consists of nine molecules: Cr_2,[27–29] V_2,[30,31] Mo_2,[28,32] Rh_2,[33] VCr,[34] VNb,[35,36] ScCo,[37] YCo,[37,38] and NbCr,[34] four of which are homonuclear bimetallics, and five of which are heteronuclear bimetallics. For seven of the molecules, both the bond length and bond energy are known experimentally, but for Rh_2, only the bond dissociation energy is known experimentally, and for VCr, only the bond length is known experimentally. Therefore, we evaluate the performance of various density functionals based on the bond lengths of eight molecules (*i.e.*, excluding Rh_2) and based on the bond dissociation energies of eight molecules (*i.e.*, excluding VCr).

3. Computational methods

All density functional calculations were carried out by finding the lowest-energy solution in order to approximate the ground electronic state, independent of symmetry. In all cases, we tried multiple initial guesses for the orbitals and for the total electron spin component M_S, and a stability analysis[39,40] was carried out to see if the solution was stable with respect to spin or symmetry breaking (except for fixing the component M_S of total electron spin and considering only collinear determinants); if the solution was unstable we broke the symmetry. In this way we tried to find the lowest-energy stable solution of the self-consistent field equations, independent of symmetry.

3.A. Converting experimental dissociation energy D_0 to D_e

The experimental equilibrium dissociation energy D_e is obtained by adding the zero-point vibrational energy (ZPE) of the diatomic molecule to the experimental ground-state dissociation energy D_0. If the experimental harmonic vibrational frequency ω_e (in units of wavenumbers) is available, then the ZPE is obtained by using the experimental ω_e scaled by a factor of 0.986, which is a generic scale factor[41] for converting a harmonic ZPE to an anharmonic one. For cases where the experimental value of ω_e is not available, we directly computed the vibrational ZPE using the M06-L XC functional with the aug-cc-pwCVTZ-DK[42] all-electron basis set and with the Douglas–Kroll–Hess 2nd order scalar relativistic Hamiltonian[43] (DKH2), and scaled by a factor of 0.985, which is the ZPE scale factor at this level of theory and is determined based on a standard database.[41] The grid size used in the DFT calculation is 99 radial shells with 974 angular points per shell.

3.B. Converting experimental bond length r_0 to r_e

The bond length measured in the experiments considered here is the vibrationally averaged ground-state bond length r_0, which is the bond length in the ground vibrational–rotational state.

Our directly computed bond lengths are equilibrium bond lengths, r_e, which correspond to the interatomic distance at the minimum of the Born–Oppenheimer potential energy curve of the diatomic molecule. For an anharmonic potential, the ground-state bond length is slightly longer than the equilibrium bond length. Next we explain how we convert the experimental r_0 to r_e in order to make an appropriate comparison.

The equilibrium rotational constant, B_e, and the rotational constant in the first vibrational state (*i.e.*, the vibrational quantum number is 0), B_0, are related by the following equation (as is commonly done, we express it in units of energy in this work):

$$B_e = B_0 + \frac{\alpha_e}{2} \quad (1)$$

where α_e is the equilibrium rotational–vibrational interaction constant. These quantities are given by

$$B_0 = \frac{h^2}{8\pi^2 \mu {r_0}^2} \quad (2)$$

and by Pekeris approximation[44]

$$\alpha_e = \frac{6\sqrt{x_e c\omega_e {B_e}^3}}{c\omega_e} - \frac{6{B_e}^2}{c\omega_e} \quad (3)$$

where h is Plank's constant, c is the speed of light, μ is the reduced mass of the diatomic molecule, ω_e is the harmonic vibrational frequency in cm^{-1}, and x_e is the anharmonicity constant. In eqn (3), the harmonic vibrational frequency ω_e is directly taken from the experimentally reported value if it is available, or it is calculated by using M06-L/aug-cc-pwCVTZ-DK with DKH2 and scaled by a factor of $\lambda^H = 0.999$, which is a scale factor (determined in this work using the method of ref. 41) for reproducing the experimental harmonic frequency from the computed harmonic vibrational frequency.

We substitute (2) and (3) into (1), and we solve the resulting equation iteratively using the Newton–Raphson method for B_e in terms of r_0, ω_e, and x_e. Then we obtain r_e from

$$r_e = \sqrt{\frac{h^2}{8\pi^2 \mu B_e}} \quad (4)$$

To do this, we obtain r_0 from the experimentally measured B_0, and ω_e has already been discussed above. To complete this process we need x_e.

Based on the assumption of a Morse potential, the anharmonicity constant x_e can be computed from D_e and ω_e (discussed above) as follows (note that, as is commonly done, we express D_e in energy units and ω_e in wave numbers):[45]

$$x_e = \frac{hc\omega_e}{4D_e} \quad (5)$$

The reference data for the diatomic molecules that we considered in the current work are shown in Table 1.

3.C. Spin–orbit coupling

The spin–orbit coupling energies for atoms are taken from the NIST collection of atomic spectroscopy data.[46] The spin–orbit coupling energies for atomic V (^{6}D), V (^{4}F), Cr (^{7}S), Mo (^{7}S), Nb (^{6}D), Rh (^{4}F), Co (^{4}F), Sc (^{2}D), and Y (^{2}D) are −0.5, −0.9, 0, 0, −1.8, −4.3, −2.3, −0.3, and −0.9 kcal mol^{-1} respectively.

For the diatomic molecules Cr_2 ($^1\Sigma$), V_2 ($^3\Sigma$), VNb ($^3\Sigma$), Mo_2 ($^1\Sigma$), ScCo ($^1\Sigma$), and YCo ($^1\Sigma$), the spin–orbit coupling energies are equal to zero because the quantum number Λ is 0. For NbCr ($^2\Delta$), Rh_2 ($^5\Delta$) and VCr ($^2\Delta$), the spin–orbit matrix elements and eigenstates were computed using the full Breit–Pauli spin–orbit operator.[47,48] In particular, state-averaged CASSCF[49,50] (SA-CASSCF) calculations without spin–orbit coupling were followed by state-interaction[51] (CAS-SI) calculations, where new eigenstates are obtained by diagonalizing the Hamiltonian with spin–orbit coupling included in a basis of the spin–orbit-free eigenfunctions. A full valence active space was used in this work, *i.e.*, the active space was CAS (11e, 12o) for NbCr, CAS (18e, 12o) for Rh_2, and CAS (11e, 12o) for VCr, respectively. The number of states in the CAS-SI calculation is the same as the number of states averaged in the SA-CASCF calculation, and it is 2 for NbCr, 40 for Rh_2, and 2 for VCr. The spin–orbit energy is then equal to the energy of the lowest CAS-SI eigenvalue minus the energy of the lowest SA-CASSCF eigenvalue. In these SA-CASSCF and CAS-SI calculations, the def2-TZVP basis set,[52] which is an all-electron basis set for the first-row transition metals, was used for Cr and V, the TZP[53] all-electron basis was used for Nb, and an ECP basis set

Table 1 Experimentally determined ground-state spin multiplicity ($2S + 1$), experimental r_0 and r_e, experimental D_0, ω_e, and D_e, and spin–orbit energy change ΔE_{SO} for the molecules in the dataset we considered in the current work. Reference values are from: Cr_2: ref. 27–29; V_2: ref. 30 and 31; Mo_2: ref. 28 and 32; Rh_2: ref. 33; VCr: ref. 34; VNb: ref. 35 and 36; ScCo: ref. 37; YCo: ref. 37 and 38; NbCr: ref. 34

Molecule	$2S+1$	Exptl r_0 (Å)	r_e (Å)	Exptl D_0 (kcal mol^{-1})	Exptl ω_e (cm^{-1})	D_e[a] (kcal mol^{-1})	ΔE_{SO}[b] (kcal mol^{-1})
Cr_2	1	1.686	1.681	35.3	480.6	36.0	0
V_2	3	—	1.770[c]	63.4	537.5	64.2	−1.8
Mo_2	1	1.941	1.938	103.2	449.0	103.9	0
Rh_2	5	—	—	55.5	—	55.9	−5.0
VCr	2	1.726	1.724	—	—	—	−0.1
VNb	3	—	1.943[c]	87.4	476.9	88.1	−2.7
ScCo	1	1.812	1.809	56.5	246.7	56.8	−2.6
YCo	1	1.983	1.980	59.7	231.3	60.0	−3.2
NbCr	2	1.894	1.892	69.8	—	70.3	−1.3

[a] Converted D_e using experimental D_0 and zero-point-energy obtained by experimental harmonic vibrational frequency ω_e (scaled by 0.986) or computed by M06-L/aug-cc-pwCVTZ-DK with DKH2 (with ZPE scale factor 0.985). [b] $\Delta E_{SO} = E_{SO}(A) + E_{SO}(B) - E_{SO}(AB)$, where $E_{SO}(X)$ is the spin–orbit coupling energy for species X. [c] For V_2 and VNb, the experimentally reported r_e values are available, and thus they are directly used.

cc-pVTZ-PP[54] including both the scalar (spin-free) relativistic effective potential (in particular ECP28MDF) and the spin–orbit potential was used for Rh. (The use of spin–orbit potentials to obtain spin–orbit couplings in nonrelativistic calculations is explained elsewhere.[55]) The computed spin–orbit coupling energies for NbCr, Rh_2 and VCr are −0.5, −3.5 and −0.4 kcal mol^{-1}, respectively.

The *Molpro* 2015.1 package[56] is used for spin–orbit coupling calculations.

3.D. B_1 diagnostics

The B_1 diagnostic,[89] which is a multireference diagnostic that is much less expensive than T_1[57] and M[58] multireference diagnostics, is computed as the difference between the equilibrium bond energy computed by BLYP and that computed by B1LYP//BLYP. The B_1 diagnostic values computed by using the def2-QZVP basis set with the SDD pseudopotential and by using the aug-cc-pwCVTZ-DK basis with the DKH2 Hamiltonian are reported in Table 2. All the B_1 diagnostic values are significantly larger than 10 kcal mol^{-1}, which is the usual criterion[89] for multireference character. These very large values indicate very large multireference character for all the molecules studied here.

3.E. Functionals

Table 3 lists the XC functionals we tested in this work along with the percentage X of the Hartree–Fock exchange in each functional. The percentage of the Hartree–Fock exchange is important because functionals with high X tend to be less accurate for multireference systems, but are often more accurate for single-reference systems. The table includes local functionals (X = 0), global hybrids (X is a global constant), and range-separated hybrids (X depends on interelectronic separation, and the range is shown in the table).

3.F. Bond dissociation energy

The equilibrium bond dissociation energy D_e is computed by broken-symmetry (BS) spin-unrestricted Kohn–Sham DFT (UKS-DFT) with various exchange–correlation (XC) density functionals.

In order to obtain the lowest-energy solution, numerous initial densities generated by various XC functionals have been tried as initial guesses for BS-UKS-DFT single-point calculations; this is an exhaustive procedure, but we certainly cannot guarantee that the global minima in the SCF solution space is reached. We always test the stability[59–61] of the computed wave function, and if an unstable wave function is obtained, we re-optimize it until a stabilized wave function is found; this procedure is carried out by using "stable = (opt, xqc)" keywords in *Gaussian 09*. The resulting broken-symmetry Slater determinant does not necessarily belong to an irreducible representation of the molecular point group, and often it does not; the Slater determinant is optimized for a specified projected component M_S of the square S^2 of the total electron spin, and, in general, the resulting Slater determinant is a mixture of different spin states rather than being a spin-eigenfunction (except for cases where the system is closed-shell or in the highest spin state for the chosen M_S). That is to say, we allow both the spatial and spin symmetry of the Slater determinant to vary, aiming to obtain the energetically lowest possible SCF solution. We remind the reader that if one had the exact exchange–correlation functional (which is unknown and probably unknowable[62]), the Slater determinant would not necessarily have the symmetry of the exact wave function,[63] and it would not necessarily be an eigenfunction of S^2. (S^2 is a two-electron operator, and expectation values requiring more than the one-electron density are not necessarily given correctly by the reference determinant.[64])

For the diatomic molecules, the DFT calculations are carried out for the spin component M_S of electron spin equal to S, where S is the experimental electron spin quantum number. For computing dissociation energies, the dissociation products (*i.e.*, the atoms) are considered to be in their ground spin state. We computed D_e as

$$D_e = E(A) + E(B) - E(AB) + \Delta E_{SO}(AB) \quad (6)$$

where $E(X)$ is the electronic energy (including nuclear repulsion) for species X, and $\Delta E_{SO}(AB)$ is the change of spin–orbit coupling energy during dissociation, which is computed as

$$\Delta E_{SO} = E_{SO}(A) + E_{SO}(B) - E_{SO}(AB) \quad (7)$$

where $E_{SO}(X)$ is the spin–orbit coupling energy for species X.

The calculation of the fourth term in eqn (6) is discussed in Section 3.C. We computed the first three terms in eqn (6) in the following four ways:

(1) SP-ECP: the def2-QZVP basis set[65] and the SDD effective core potential (ECP)[66] are used to compute single-point (SP) energies at the experimental geometry;

(2) SP-DKH: the all-electron aug-cc-pwCVTZ-DK basis is used with the DKH2 Hamiltonian to compute single-point energies at the experimental geometry;

(3) opt-ECP: the same basis and ECP as for SP-ECP, but the geometry is optimized at the same level.

(4) opt-DKH: the same basis and Hamiltonian as for SP-DKH, but the geometry is optimized at the same level.

DFT calculations were carried out using locally modified *Gaussian 09*[67] with a grid size of 974 angular points per shell and 99 radial shells. In some cases, the geometry optimization was carried out with analytic gradients and in other cases by scanning the potential energy curve.

3.G. Analysis of electronic structures

In order to further understand the performance of various density functionals, we used the keyword "pop = (NOAB, Hirshfeld)" in

Table 2 Computed B_1 diagnostic values (kcal mol^{-1})

Molecule	B_1 (def2-QZVP basis and SDD ECP)	B_1 (aug-cc-pwCVTZ-DK basis and DKH2 Hamiltonian)
Cr_2	57.2	56.9
V_2	65.6	78.2
Mo_2	43.5	44.7
Rh_2	36.7	41.5
VCr	66.8	62.7
VNb	51.2	57.6
ScCo	59.9	69.4
YCo	51.5	61.6
NbCr	43.9	47.8

Table 3 Exchange–correlation (XC) functionals tested in this work

Type	XC functional	X^a	Ref.
GGA	PBEsol	0	84
	SOGGA	0	85
	SOGGA11	0	86
	BLYP	0	87 and 88
	MOHLYP	0	89
	OLYP	0	90
	OreLYP	0	91
	PBE	0	92
	revPBE	0	93
	RPBE	0	94
NGA	GAM	0	95
	N12	0	96
meta-GGA	M06-L	0	97
	M11-L	0	98
	MGGA_MS0	0	99
	MGGA_MS1	0	99
	MGGA_MS2	0	99
	τ-HCTH	0	100
meta-NGA	MN12-L	0	101
	MN15-L	0	102
Global-hybrid GGA	B1LYP	25	103
	B3LYP	20	104
	B97-1	21	105
	B97-3	26.93	106
	MPW1B95	31	107
	MPW1K	42.8	108
	MPW3LYP	21.8	109
	MPWB1K	44	107
	O3LYP	11.61	110
	PBE0	25	111
	SOGGA11-X	40.15	112
Global-hybrid meta-GGA	MGGA_MS2h	9	99
	M05	28	113
	M05-2X	56	114 and 115
	M06	27	116 and 117
	M06-2X	54	114 and 117
	M06-HF	100	118
	M08-HX	56.79	115
	M08-SO	52.23	115
	PW6B95	28	119
	PWB6K	46	119
	TPSSh	10	120
	τ-HCTHhyb	15	121
Global-hybrid meta-NGA	MN15	44	122
Range-separated hybrid GGA	HSE06	25–0	123 and 124
	ωB97X	15.77–100	125
Range-separated hybrid GGA + MM[b]	ωB97X-D	22.2–100	126
Range-separated hybrid meta-GGA	M11	42.8–100	127
Screened-exchange NGA	N12-SX	25–0	128
Screened-exchange meta-NGA	MN12-SX	25–0	128

[a] X is the percentage of nonlocal Hartree–Fock exchange. When a range is given, the first value is for small interelectronic distances, and the second is for large interelectronic distances. [b] MM denotes the addition of molecular mechanics (also called an empirical dispersion correction), which in this case corresponds to atom–atom pairwise damped dispersion terms added post-SCF to the calculated energy.

Gaussian 09 to perform natural orbital analysis and Hirshfeld population analysis for the α and β densities of the final broken-symmetry solution. We also carried out CASSCF calculations to investigate the dominant configurations and their relative contributions in the total wave function of the diatomic molecules; and since we are aiming at this part of the work to acquire a qualitative understanding, a full-valence active space was deemed sufficient. The ANO-RCC-VTZP basis set and the DKH2 Hamiltonian are used in the CASSCF calculations; all of these calculations are performed by using Molcas 8.1[68] at the

experimental equilibrium geometry (except for Rh_2, whose experimental bond length is unavailable, and so we use the BLYP predicted r_e, which is 2.234 Å).

4. Results

As indicated above, not only do we test 50 XC functionals, but we also compare the accuracy of using a valence basis set combined with an effective core potential (this combination is simply denoted as "ECP" in this paper) to that obtained using an all-electron basis with the DKH2 Hamiltonian (simply denoted as "DKH"). In the article, we tabulated the results for the twelve XC functionals with the smallest mean unsigned errors in each case; full tabulations of the results are given in the ESI.†

4.A. Equilibrium bond length

Table 4 lists the signed errors and mean unsigned errors (MUEs) for the computed equilibrium bond lengths using various XC functionals, with the ECP protocol; the results for the DKH protocol are in Table 5.

For the ECP calculations, the functional that gives the smallest mean unsigned error (MUE) for the computed equilibrium bond length of the eight diatomic molecules is BLYP, whose MUE is 0.029 Å. The functionals that give an MUE smaller than 0.05 Å are BLYP, MN12-L, MGGA_MS1, RPBE, SOGGA11, revPBE, MGGA_MS2, PBE, MOHLYP, MGGA_MS0, OreLYP, M06-L, and OLYP. The best functionals for predicting the bond length for specific molecules are as follows: Mo_2 and YCo, BLYP; Cr_2, PW6B95; V_2, SOGGA11-X; VCr, MGGA_MS1; VNb, MPWB1K; ScCo, MN12-L; and NbCr, M06; and the unsigned errors of these best predictions range from 0.001 Å for YCo to 0.015 Å and 0.062 Å, respectively, for the notoriously difficult V_2 and Cr_2.

For the DKH calculations, the best functional (on average) for the computed equilibrium bond length is still BLYP, for which the MUE now is reduced by more than a factor of four to 0.007 Å. The functionals that give an MUE smaller than 0.05 Å are BLYP, RPBE, revPBE, SO11, PBE, MOHLYP, OLYP, OreLYP, PBEsol and MGGA_MS0. The best functionals for predicting the bond length for specific molecules are as follows: Cr_2, Mo_2, VNb, and NbCr, BLYP; YCo and ScCo, SOGGA11; V_2, MGGA_MS2; and VCr, revPBE; and the unsigned errors of these best predictions range from 0.000 Å for V_2, VCr, and NbCr to 0.006 Å for VNb.

The improvement, compared to the ECP results, in the very best DKH results (MUE of best performing functional and smallest MUEs for individual molecules) is dramatic, but the decrease in the number of functionals with an MUE below 0.05 Å from 13 to 10 is disappointing. In fact, upon changing from the ECP protocol to the DKH one, the MUEs of almost half of the functionals we tested become larger – sometimes dramatically; for example, the MUE for M11 increases from 0.116 Å to 0.304 Å, and that for MPW3LYP increases from 0.080 Å to 0.270 Å. Only four functionals (BLYP, RPBE, SOGGA11, and revPBE) have an MUE below 0.04 Å for both the ECP and DKH protocols. Clearly further work is needed to obtain ECPs that mimic DKH calculations.

Some popular functionals do very poorly. For example, the MUEs for PBE0 are 0.176 Å (ECP) and 0.124 Å (DKH), and those for B3LYP are 0.077 Å (ECP) and 0.135 Å (DKH).

4.B. Prediction of equilibrium internuclear distance for Rh_2

The experimental r_e for Rh_2 molecule is unknown, because the rotational constant is quite small and the high spin of the molecule (quintet) causes each rotational level to split into five sublevels. Therefore, the rotationally resolved spectrum for Rh_2 would be difficult to analyze. Based on the benchmark, here we give the computed r_e for Rh_2. Our result for the r_e of Rh_2 using the methods that do best in our validation study are 2.234, 2.180 and 2.361 Å by BLYP, MN12-L and MGGA_MS1 using the ECP protocol and 2.234, 2.223 and 2.219 Å by BLYP, RPBE and revPBE using the DKH protocol. Taking the average of these six values as our best validated prediction gives 2.24 Å with a standard deviation of 0.06 Å. This indicates that the MGGA_MS1 (ECP) value is an outlier because it differs from the average by two standard deviations. We therefore refine our prediction based on the other five values, which yields 2.22 Å with a standard deviation of 0.02 Å.

4.C. Equilibrium bond dissociation energy

The signed errors and mean unsigned errors of D_e, by the four ways of computation (see Section 3.F), are given in Tables 6–9.

Table 4 The signed errors and mean unsigned errors (MUEs) for the calculated equilibrium bond length (r_e in the units of Å) for the best 12 XC functionals in this category, using the ECP protocol

Functional	Cr_2	V_2	Mo_2	VCr	VNb	ScCo	YCo	NbCr	MUE
BLYP	−0.083	−0.040	−0.007	−0.055	−0.019	−0.028	−0.001	0.003	0.029
MN12-L	−0.100	−0.019	−0.021	0.064	−0.008	−0.011	−0.002	0.048	0.034
MGGA_MS1	−0.106	−0.031	−0.031	0.003	−0.034	−0.045	−0.026	0.012	0.036
RPBE	−0.092	−0.048	−0.021	−0.004	−0.031	−0.037	−0.012	−0.049	0.037
SOGGA11	−0.100	−0.053	−0.041	−0.015	−0.042	−0.035	−0.006	−0.004	0.037
revPBE	−0.093	−0.050	−0.022	−0.006	−0.032	−0.039	−0.015	−0.049	0.038
MGGA_MS2	−0.103	−0.037	−0.026	−0.043	−0.030	−0.044	−0.021	0.012	0.039
PBE	−0.096	−0.054	−0.025	−0.068	−0.037	−0.046	−0.024	−0.004	0.044
MOHLYP	−0.101	−0.057	−0.035	0.011	−0.042	−0.041	−0.013	−0.058	0.045
MGGA_MS0	−0.107	−0.106	−0.031	0.012	−0.032	−0.045	−0.026	0.017	0.047
OreLYP	−0.108	−0.066	−0.040	−0.013	−0.051	−0.060	−0.037	−0.005	0.048
M06-L	−0.106	−0.061	−0.046	0.005	−0.044	−0.054	−0.039	0.027	0.048
Exptl r_e	1.681	1.770	1.938	1.724	1.943	1.809	1.980	1.892	—

Table 5 The signed errors and mean unsigned errors (MUEs) for the calculated equilibrium bond length (r_e in the units of Å) for the best 12 XC functionals in this category, using the DKH protocol

Functional	Cr_2	V_2	Mo_2	VCr	VNb	ScCo	YCo	NbCr	MUE
BLYP	0.003	−0.018	−0.003	−0.015	−0.006	−0.005	0.007	0.000	0.007
RPBE	−0.085	−0.024	−0.020	0.006	−0.017	−0.011	−0.005	0.013	0.023
revPBE	−0.087	−0.026	−0.021	0.000	−0.019	−0.014	−0.008	0.012	0.024
SOGGA11	0.028	−0.021	−0.040	−0.039	−0.067	0.002	0.003	0.002	0.025
PBE	−0.092	−0.033	−0.024	−0.023	−0.025	−0.025	−0.018	−0.005	0.031
MOHLYP	−0.095	−0.032	−0.035	0.062	−0.028	−0.010	−0.006	−0.036	0.038
OLYP	0.096	−0.048	−0.043	−0.012	−0.042	−0.037	−0.032	−0.001	0.039
OreLYP	0.120	−0.048	−0.042	−0.009	−0.041	−0.038	−0.033	−0.004	0.042
PBEsol	−0.105	−0.049	−0.036	−0.053	−0.040	−0.048	−0.042	−0.008	0.048
MGGA_MS0	−0.106	−0.109	−0.039	0.009	−0.035	−0.035	−0.040	0.018	0.049
SOGGA	−0.107	−0.051	−0.040	−0.052	−0.043	−0.050	−0.045	−0.032	0.053
τ-HCTH	−0.122	−0.066	−0.050	−0.024	−0.056	−0.057	−0.047	−0.009	0.054
Exptl r_e	1.681	1.770	1.938	1.724	1.943	1.809	1.980	1.892	—

Table 6 The signed errors and mean unsigned errors (MUEs) for the calculated equilibrium bond dissociation energy ($D_e^{SP\text{-}ECP}$ in the units of kcal mol^{-1}) for the best 12 XC functionals in this category, using the def2-QZVP basis combined with the SDD ECP

Functional	Cr_2	V_2	Mo_2	Rh_2	VNb	ScCo	YCo	NbCr	MUE
τ-HCTHhyb	2.1	0.1	8.4	5.0	−0.2	7.9	−11.0	−6.2	5.1
M05	−5.7	9.1	9.0	1.5	7.8	12.1	−12.5	−1.7	7.4
MN15	−9.0	13.0	−11.4	2.8	−2.0	12.6	−9.9	−13.6	9.3
M06-L	14.0	22.9	−6.9	9.3	10.5	23.6	−3.9	−4.8	12.0
BLYP	9.2	25.1	4.5	11.0	8.8	30.8	6.5	−2.3	12.3
N12-SX	−0.6	−24.3	3.3	−3.1	−14.5	−19.0	−32.8	−2.0	12.4
M06	−10.1	15.7	2.2	10.1	11.0	10.3	−14.4	−29.3	12.9
OreLYP	2.3	26.6	−1.4	10.3	10.3	39.0	12.7	−12.3	14.4
MN15-L	−14.0	1.8	−33.0	5.0	−14.1	20.6	−2.7	−24.4	14.5
RPBE	−6.4	31.7	−19.7	4.8	3.9	30.9	5.8	−15.3	14.8
OLYP	−2.0	28.2	−10.6	5.8	5.7	37.3	10.9	−18.8	14.9
O3LYP	−23.9	−0.8	−27.6	−10.1	−16.5	11.2	−11.2	−29.2	16.3
Exptl D_e	36.0	64.2	103.9	55.9	88.1	56.8	60.0	70.3	—

Table 7 The signed errors and mean unsigned errors (MUEs) for the calculated equilibrium bond dissociation energy ($D_e^{SP\text{-}DKH}$ in the units of kcal mol^{-1}) for the best 12 XC functionals in this category, using the aug-cc-pwCVTZ-DK all-electron basis and DKH2

Functional	Cr_2	V_2	Mo_2	Rh_2	VNb	ScCo	YCo	NbCr	MUE
τ-HCTHhyb	0.2	−4.9	4.0	10.8	−0.3	4.6	−5.0	1.6	3.9
M06-L	−3.3	−8.0	−16.9	−7.2	−8.8	9.9	−4.6	−5.6	8.0
N12-SX	11.8	−14.1	5.7	−0.9	−6.1	−11.3	−17.8	−2.1	8.7
OreLYP	0.3	16.3	−1.7	10.5	7.3	24.8	13.0	−1.1	9.4
GAM	−7.6	4.6	−19.4	12.5	−4.4	20.6	6.3	−10.8	10.8
OLYP	−5.6	17.1	−11.3	6.4	2.3	23.9	11.6	−16.1	11.8
MN12-L	21.6	−16.7	−6.8	−16.9	−17.8	−4.2	−13.3	1.7	12.4
RPBE	−6.4	23.5	−21.5	5.9	1.7	22.7	10.7	−17.3	13.7
M05	−16.7	−19.5	−10.7	−6.3	−12.8	−11.0	−23.1	−11.9	14.0
BLYP	14.4	25.1	5.5	13.1	11.4	26.9	13.0	7.1	14.6
revPBE	−7.4	26.1	−22.1	6.9	2.6	24.8	12.6	−18.1	15.1
TPSSh	−25.5	−5.0	−32.0	−9.1	−17.9	−1.8	−10.3	−26.3	16.0
Exptl D_e	36.0	64.2	103.9	55.9	88.1	56.8	60.0	70.3	—

First, we compare the bond energies computed based on experimental geometry to those based on optimized geometries, *i.e.*, we compare D_e by SP-ECP to D_e by opt-ECP and D_e by SP-DKH to D_e by Opt-DKH. For both SP-ECP and Opt-ECP, the best five functionals for D_e are τ-HCTHhyb, M05, MN15, M06-L and BLYP; for SP-ECP, their MUEs are respectively 5.1, 7.4, 9.3, 12.0, and 12.3 kcal mol^{-1}, and for Opt-ECP, they are 6.7, 10.3, 11.9, 11.7, and 11.8 kcal mol^{-1}. For SP-DKH and Opt-DKH, the best four functionals are τ-HCTHhyb, M06-L, N12-SX and OreLYP, all of which have MUEs smaller than 10 kcal mol^{-1}. The fifth best functional for SP-DKH is GAM (MUE = 10.8 kcal mol^{-1}) and for Opt-DKH it is OLYP (MUE = 12.0 kcal mol^{-1}). Thus, the conclusions about what are the best performing functionals are not sensitive to the choice between calculated and experimental geometries. Generally, for a given functional, the difference between the MUEs of SP and Opt calculations is smaller

Table 8 The signed errors and mean unsigned errors (MUEs) for the calculated equilibrium bond dissociation energy ($D_e^{opt\text{-}ECP}$ in the units of kcal mol^{-1}) for the best 12 XC functionals in this category, using the def2-QZVP basis combined with the SDD ECP

Functional	Cr_2	V_2	Mo_2	Rh_2	VNb	ScCo	YCo	NbCr	MUE
τ-HCTHhyb	−11.1	−7.7	7.0	5.1	0.5	9.5	−10.3	−1.9	6.7
M05	−20.4	12.6	8.6	2.9	10.6	14.0	−11.9	−1.7	10.3
M06-L	6.4	25.0	−7.8	9.3	11.3	24.6	−3.6	5.9	11.7
BLYP	5.1	25.9	4.5	11.0	9.0	31.0	6.5	1.1	11.8
MN15	−20.0	21.0	−14.6	1.7	−0.2	16.2	−8.6	−13.2	11.9
M06	−25.6	18.6	1.7	10.8	12.2	12.4	−13.5	−8.5	12.9
N12-SX	−13.7	−24.8	1.5	−3.0	−14.7	−17.4	−32.0	−4.2	13.9
OreLYP	−5.0	29.0	−1.9	10.3	11.4	40.2	13.0	−3.5	14.3
OLYP	−8.6	30.7	−11.4	5.9	6.9	38.4	11.3	−10.2	15.4
RPBE	−12.0	33.0	−20.3	4.8	4.3	31.3	5.8	−16.2	16.0
GAM	−18.4	21.0	−6.6	15.6	7.3	42.8	15.8	−6.0	16.7
revPBE	−12.8	35.1	−21.2	5.8	4.9	32.9	7.3	−17.1	17.1
Exptl D_e	36.0	64.2	103.9	55.9	88.1	56.8	60.0	70.3	—

Table 9 The signed errors and mean unsigned errors (MUEs) for the calculated equilibrium bond dissociation energy ($D_e^{opt\text{-}DKH}$ in the units of kcal mol^{-1}) for the best 12 XC functionals in this category, using the aug-cc-pwCVTZ-DK all-electron basis and DKH2

Functional	Cr_2	V_2	Mo_2	Rh_2	VNb	ScCo	YCo	NbCr	MUE
τ-HCTHhyb	10.4	−3.1	2.4	10.9	0.2	5.5	−4.4	−21.5	7.3
N12-SX	10.9	−14.4	4.2	−1.4	−9.5	−10.5	−17.3	2.3	8.8
M06-L	−14.3	−7.2	−18.9	−9.2	−8.4	10.3	−4.4	−4.1	9.6
OreLYP	1.4	17.3	−2.0	10.5	8.0	25.2	13.3	−1.1	9.8
OLYP	−4.8	18.1	−11.9	6.4	3.0	24.3	11.8	−16.1	12.0
MN12-L	21.7	−17.5	−8.8	−16.1	−22.2	−3.1	−12.6	3.2	13.2
RPBE	−10.3	23.8	−22.1	5.9	1.8	22.8	10.7	−17.8	14.4
BLYP	14.4	25.2	5.5	13.2	11.4	27.0	13.0	7.1	14.6
GAM	−20.5	5.9	−22.8	12.2	−3.7	20.9	6.5	−26.9	14.9
M05	−33.8	−16.8	−13.2	−6.3	−10.8	−10.6	−22.7	−11.2	15.7
revPBE	−11.1	26.4	−22.6	6.9	2.8	24.8	12.6	−18.6	15.7
B97-1	1.1	−26.4	−12.1	−4.7	−21.3	−21.3	−27.2	−16.7	16.4
Exptl D_e	36.0	64.2	103.9	55.9	88.1	56.8	60.0	70.3	—

than 5 kcal mol^{-1}; and on average (*i.e.*, averaged over all the functionals), this difference is only 2.6 kcal mol^{-1} for the ECP protocol and only 3.2 kcal mol^{-1} for the DKH one.

Next, we compare ECP and DKH options for given functionals. For the functional that performs best for dissociation energies, *i.e.*, τ-HCTHhyb, the MUE of SP-ECP is 1.2 kcal mol^{-1} larger than the MUE of SP-DKH; but the MUE of opt-ECP is 0.6 kcal mol^{-1} smaller than the MUE of opt-DKH. For half of the functionals, the differences of the MUEs given by ECP from DKH options are smaller than 5 kcal mol^{-1}. For some functionals, such as M08-SO, M06-2X, and MN15, using an ECP is significantly better than using an all-electron DKH calculation. On the other hand, for MN12-L, the all-electron DKH calculation is more accurate than the ECP one, both for calculations at the experimental geometry and for those at consistently optimized geometries. As might be expected from these examples, the conclusions about whether one functional performs better than another are not the same if based on ECP or DKH calculations. One can make the generalization that hybrid functionals tend to perform better when ECP basis is used and local functionals seem to be more accurate when all-electron relativistic calculations are performed; and this finding is also observed in one previous study on 3d transition metal systems.[69]

4.D. Prediction of the equilibrium dissociation energy for VCr

The bond energy of VCr is not known experimentally, but we can predict it here by using the density functionals that perform best for bond dissociation energies. In particular, the τ-HCTHhyb functional is found to be the best XC functional for both ECP and all-electron relativistic calculations with DKH. The D_e given by τ-HCTHhyb with an optimized bond length is 51.0 kcal mol^{-1} with the ECP protocol and 54.7 kcal mol^{-1} with DKH; on average, these predictions give an equilibrium bond dissociation energy of 52.9 kcal mol^{-1}. This is very close to the equilibrium bond energy predicted in a previous theoretical study[70] using multi-state CASPT2, which yields 52.2 kcal mol^{-1}.

4.E. Assessment of the performance of various XC functionals

We rank the performance of various XC functionals based on their MUEs in each category in Table 10. The overall ranking is determined based on the average ranking of all the categories. Based on this overall ranking, nine functionals, in particular, BLYP, RPBE, M06-L, OreLYP, N12-SX, OLYP, revPBE, τ-HCTHhyb, and M05, have single-digit average ranks when averaged over all six columns. However, if one already has the experimentally determined structures, one can obtain single-point energies, and when averaged over only those two columns, again there

Table 10 Rankings of the performances of various XC density functionals, combined across both ways of computing r_e and all four ways of computing D_e

Functional	X	r_e ECP	r_e DKH	D_e SP-ECP	D_e SP-DKH	D_e opt-ECP	D_e opt-DKH	Overall
BLYP	0	1	1	5	10	4	8	1
RPBE	0	4	2	10	8	10	7	2
M06-L	0	12	18	4	2	3	3	3
OreLYP	0	11	8	8	4	8	4	4
N12-SX	≤25	19	13	6	3	7	2	5
OLYP	0	13	7	11	6	9	5	6
revPBE	0	6	3	14	11	12	11	7
τ-HCTHhyb	15	27	30	1	1	1	1	8
M05	28	29	25	2	9	2	10	9
PBE	0	8	5	20	15	19	14	10
MOHLYP	0	9	6	16	18	16	17	11
M06	27	30	26	7	14	6	18	12
MGGA_MS2	0	7	24	23	16	21	13	13
SOGGA11	0	5	4	21	24	22	28	14
MN12-L	0	2	14	42	7	40	6	15
GAM	0	42	32	13	5	11	9	16
O3LYP	11.61	22	33	12	13	15	19	17
MN15-L	0	23	36	9	20	13	15	18
MGGA_MS1	0	3	17	28	21	28	23	19
B97-1	21	26	37	15	17	14	12	20
MGGA_MS0	0	10	10	27	23	27	24	21
SOGGA	0	16	11	25	26	23	25	22
PBEsol	0	15	9	26	27	24	26	23
TPSSh	10	33	31	17	12	18	16	24
M11-L	0	21	15	22	19	29	22	25
N12	0	18	16	18	30	17	29	26
MN15	44	38	46	3	25	5	27	27
MN12-SX	≤25	32	20	29	22	25	20	28
B3LYP	20	25	29	24	28	26	30	29
MPW3LYP	21.8	28	47	19	29	20	21	30
B97-3	26.93	24	19	30	32	31	37	31
PW6B95	28	41	21	31	31	30	34	32
τ-HCTH	0	17	12	48	35	45	33	33
ωB97X-D	≥22.2	34	23	34	34	33	35	34
MGGA_MS2h	9	14	28	39	38	38	39	35
ωB97X	≥15.77	39	34	32	33	32	32	36
B1LYP	25	20	35	38	39	39	38	37
PBE0	25	44	27	37	37	36	40	38
HSE06	≤25	40	40	36	36	34	36	39
MPW1B95	31	43	44	33	40	35	31	40
SOGGA11-X	40.15	31	22	44	43	44	44	41
M08-SO	52.23	36	38	35	49	37	49	42
M05-2X	56.79	47	39	40	41	41	43	43
M11	≥42.8	37	48	45	42	47	41	44
M06-2X	54	46	42	41	44	42	48	45
MPWB1K	44	45	41	43	46	43	46	46
MPW1K	42.8	35	45	50	48	49	47	47
M08-HX	56.79	48	43	47	47	48	45	48
PWB6K	46	49	50	46	45	46	42	49
M06-HF	100	50	49	49	50	50	50	50

are nine functionals with single-digit ranks, with GAM replacing RPBE on the above list. If one considers only the prediction of the geometry (*i.e.*, of the equilibrium internuclear distance), the functionals with single-digit average ranks are BLYP, RPBE, SOGGA11, revPBE, PBE, MOHLYP, MN12-L, and OreLYP. If we only consider the homonuclear bimetallic bonds tested in this work, BLYP, MN12-L, and SOGGA11 give the best bond lengths, and their mean unsigned errors (averaged over both ECP and DKH approaches) are respectively 0.025, 0.046, and 0.047 Å; and τ-HCTHhyb, N12-SX, and OreLYP give the best bond energies, and their mean unsigned errors (averaged over all of the four approaches for computing D_e) are respectively 5.8, 8.6, and 9.2 kcal mol^{-1}. This order is consistent with the trend of considering the performance of functionals for the whole test set.

A somewhat surprising result of the present study is the sometimes very large difference in predictions when using ECPs and when using all-electron calculations. One might be tempted to conclude that one should not use ECPs except for the fact that, on average, the results with ECPs are more accurate. An interesting contrast is that the performance of M06-L is not sensitive to whether one uses an ECP basis or an all-electron aug-cc-pwCVTZ-DK basis with DKH2, but for MN15, the ECP basis tends to give better results than the aug-cc-pwCVTZ-DK basis with the DKH2 Hamiltonian. The situation regarding ECPs and DKH calculations needs further study.

Generally, local functionals show better performances for predicting the bond lengths, while some hybrid functionals, such as τ-HCTHhyb, M05, M06, N12-SX, and MN15 (when used

with an ECP), are able to provide reasonably accurate bond energies. The meta-GGA functionals and the hybrid meta-GGA functionals with small or moderate amounts of Hartree–Fock exchange generally have good performances. This means adding kinetic energy density (*i.e.*, τ) into the XC density functional can improve its performance, and this could be attributed to the ability of kinetic energy density to recognize the slowly varying electron density and to distinguish various types of chemical bonds.[71–73] Hybrid density functionals with large amounts of Hartree–Fock exchange fail even qualitatively – this is not surprising since it was pointed out in the original papers for functionals like M08-HX, M08-SO, and M06-2X that – because functionals with high Hartree–Fock exchange were already known to perform poorly for molecules containing transition metals – they were not optimized for (and hence not recommended for) transition metal chemistry, although they show excellent performance for main-group chemistry. The only functionals in the top 50%-ile in the overall average rank (Table 10) that have nonzero Hartree–Fock exchange are N12-SX (25% at small interelectronic separation, decreasing to zero as interelectronic separation increases), τ-HCTHhyb (15%), M05 (28%), M06 (27%), O3LYP (11.61%), B97-1 (21%), and TPSSh (10%). The physical reason for the poor performance when Hartee–Fock exchange is included is the static correlation error[74] brought in by the Hartree–Fock exchange.

Over 60% of the density functionals we tested here have average unsigned errors larger than 20 kcal mol^{-1} for predicting the bond energies, and the majority of the density functionals cannot give the bond lengths (on average) better than 0.08 Å. Only two functionals (M06-L and OreLYP) can give MUEs smaller than 10 kcal mol^{-1} for bond energies and also give MUEs smaller than 0.05 Å for bond lengths. The N12-SX functional can also give bond energies better than 10 kcal mol^{-1}, but with slightly larger average errors in bond lengths. This situation clearly exposes the limitations of the current exchange–correlation functionals for metal–metal bonds with a highly multireference character.

5. Analysis

5.A. Broken-symmetry solution of V_2

In this section, we first discuss the broken-symmetry UKS-DFT solution of the V_2 molecule, which is chosen as an example to illustrate some characteristics of the broken-symmetry calculation. The CASSCF calculation shows that the dominant configuration (which contributes 71% to the total wave function) of V_2 is

$$\left(\sigma_{3d_{z^2}}\right)^2(\sigma_{4s})^2(\pi_{3d_{xz}})^2(\pi_{3d_{yz}})^2\left(\delta_{3d_{x^2-y^2}}\right)^1(\delta_{3d_{xy}})^1,$$

where the two σ orbitals are actually $3d_{z^2}$ and 4s hybridized; the second most important configuration, which has a contribution of 3%, is

$$\left(\sigma_{3d_{z^2}}\right)^2(\sigma_{4s})^2(\pi_{3d_{xz}})^2(\pi_{3d_{yz}})^2\left(\delta_{3d_{x^2-y^2}}{}^*\right)^1(\delta_{3d_{xy}}{}^*)^1,$$

The CASSCF wave function is a $^3\Sigma_g^-$ state, where "g" indicates that the total electronic wave function is symmetric with respect to the inversion center (the direct product of the two delta orbitals of the dominant configuration is g × g = g), and "−" indicates that the total wave function changes its sign under reflection in the *yz* mirror plane (the *z* axis is along the bond) because the direct product of the two delta orbitals "+"×"−" = "−". However, the symmetry of the electronic state of a broken-symmetry UKS-DFT wave function cannot be assigned in this way; the symmetry elements (such as inversion center or *yz* mirror plane) can be absent in the BS-UKS wave function. This illustrates a key aspect of the BS calculation, namely the breaking of the spatial symmetry. We will further illustrate this by comparing the shape of the BS-UKS orbitals and the CASSCF orbitals.

For the τ-HCTHhyb functional, which performs the best for this molecule (also it is the best in general), we compare the KS orbitals from three different SP-ECP calculations (single-point calculations at the experimental bond length with the ECP basis): (1) UKS calculation with the mixed HOMO and LUMO as the initial guess, but not using "stab = opt" to further break the symmetry in order to find the stable SCF solution; (2) BS-UKS calculation using "stab = opt" and the same initial guess in (1); and (3) the calculation that we actually used in computing the bond energy in this paper, *i.e.*, a BS-UKS calculation using "stab = opt" and where we also varied the initial guess (where various initial guesses were generated by different preliminary UKS calculations) in order to find the lowest-energy stabilized SCF solution. Calculation (3) yields the lowest electronic energy; it is 4.8 kcal mol^{-1} lower than the solution from calculation (2), and it is 17.8 kcal mol^{-1} lower than calculation (1).

Next, we compare the shape of some of the KS orbitals obtained from calculations (1), (2) and (3), with the CASSCF orbitals, which are shown in Fig. 1; orbitals from different calculations but with nearly indistinguishable shape are omitted from discussion here. As we can see from Fig. 1, the CASSCF orbitals have well-defined symmetries; all of the three plotted orbitals have an inversion center and *xy* and *yz* mirror planes. The KS orbitals from calculation (1) are very similar to the CASSCF orbitals, and they also have the symmetry elements mentioned above. However, the spatial symmetries are significantly distorted in the KS orbitals generated from calculations (2) and (3). The inversion center and the *xy* mirror plane are lost in the $\delta_{3d_{x^2-y^2}}$, and $\delta_{3d_{x^2-y^2}}{}^*$ orbitals of both (2) and (3), while in (2), the *yz* mirror plane is still present; these two orbitals are further twisted in (3) and the *yz* mirror plane no longer exists. Although these significantly broken-symmetry orbitals are clearly δ-like orbitals, the symmetry of the Slater determinant of the BS-UKS-DFT solution is no longer well defined.

Another aspect of broken-symmetry solutions is that the resulting wave function is not necessarily a spin-eigenfunction; it mixes multiple electronic configurations in order to produce an optimal electron density for a multireference system by using a single Slater determinant. The computed $\langle S^2\rangle$ values for calculations (1), (2), and (3) are, respectively, 2.00, 2.94, and 2.01, while the pure triplet state would have $\langle S^2\rangle = 2$. For the BS solution of other functionals, this spin-contamination is sometimes more severe; for instance, MPW1K gives $\langle S^2\rangle = 3.80$, which significantly

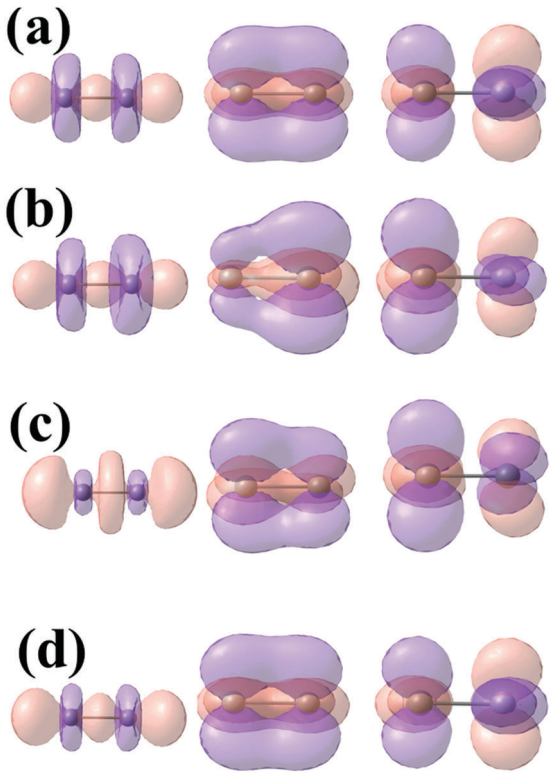

Fig. 1 (a) KS orbitals of V_2 yielded from calculation (1), (b) from calculation (2), (c) from calculation (3); (d) CASSCF orbitals. From left to right are, respectively, $\sigma_{3d_{z^2}}$, $\delta_{3d_{x^2-y^2}}$, and $\delta_{3d_{x^2-y^2}}{}^*$ orbitals. Please see Section 5.A for the definitions of calculations (1) to (3). All of the orbitals are plotted with the same contour value of 0.40.

mixes in some quintuple state character. Although such "spin contamination" is considered by many workers to be a flaw in KS-DFT, we view it otherwise. This is the way that KS-DFT works; this is the way it optimizes the orbitals to try to represent the accurate density of a multireference system by a single Slater determinant.

5.B. Electronic configurations

In this subsection, we compare the dominant electronic configurations of the CASSCF calculations to the configurations of the optimized DFT Slater determinants.

5.B.1. Mo_2, ScCo, YCo, and Cr_2. The ground states of all four of these diatomics are open-shell singlets. For Mo_2, the dominant configuration given by the CASSCF wave function is

$$\left(\sigma_{4d_{z^2}}\right)^2(\sigma_{5s})^2(\pi_{4d_{xz}})^2(\pi_{4d_{yz}})^2\left(\delta_{4d_{x^2-y^2}}\right)^2(\delta_{4d_{xy}})^2,$$

which contributes 66% to the total wave function; the next two equally important configurations are

$$\left(\sigma_{4d_{z^2}}\right)^2(\sigma_{5s})^2(\pi_{4d_{xz}})^2(\pi_{4d_{yz}})^2(\delta_{4d_{xy}})^2\left(\delta_{4d_{x^2-y^2}}{}^*\right)^2,$$

and

$$\left(\sigma_{4d_{z^2}}\right)^2(\sigma_{5s})^2(\pi_{4d_{xz}})^2(\pi_{4d_{yz}})^2\left(\delta_{4d_{x^2-y^2}}\right)^2(\delta_{4d_{xy}}{}^*)^2,$$

each of which contributes 3.5%. For ScCo, the dominant configuration of the CASSCF wave function is

$$\left(\sigma_{3d_{z^2}}\right)^2(\sigma_{4s})^2(\pi_{3d_{xz}})^2(\pi_{3d_{yz}})^2\left(\delta_{3d_{x^2-y^2}}\right)^2(\delta_{3d_{xy}})^2,$$

which contributes 81% to the total wave function; the next important configuration is

$$(\sigma_{4s})^2(\pi_{3d_{xz}})^2(\pi_{3d_{yz}})^2\left(\delta_{3d_{x^2-y^2}}\right)^2(\delta_{3d_{xy}})^2\left(\sigma_{3d_{z^2}}{}^*\right)^2,$$

which contributes 1.5%. For YCo, the dominant configuration of the CASSCF wave function is

$$\left(\sigma_{3d_{z^2}-4d_{z^2}}\right)^2(\sigma_{4s-5s})^2(\pi_{3d_{xz}-4d_{xz}})^2(\pi_{3d_{yz}-4d_{yz}})^2\left(\delta_{3d_{x^2-y^2}-4d_{x^2-y^2}}\right)^2 \times (\delta_{3d_{xy}-4d_{xy}})^2,$$

which contributes 80% to the total wave function; the next important configuration is

$$(\sigma_{4s-5s})^2(\pi_{3d_{xz}-4d_{xz}})^2(\pi_{3d_{yz}-4d_{yz}})^2\left(\delta_{3d_{x^2-y^2}-4d_{x^2-y^2}}\right)^2(\delta_{3d_{xy}-4d_{xy}})^2 \times \left(\sigma_{3d_{z^2}-4d_{z^2}}{}^*\right)^2,$$

which contributes 3.5%. For Cr_2, the dominant configuration given by the CASSCF wave function is

$$\left(\sigma_{3d_{z^2}}\right)^2(\sigma_{4s})^2(\pi_{3d_{xz}})^2(\pi_{3d_{yz}})^2\left(\delta_{3d_{x^2-y^2}}\right)^2(\delta_{3d_{xy}})^2,$$

which contributes 47% to the total wave function; the next two equally important configurations are

$$\left(\sigma_{3d_{z^2}}\right)^2(\sigma_{4s})^2(\pi_{3d_{xz}})^2(\pi_{3d_{yz}})^2(\delta_{3d_{xy}})^2\left(\delta_{3d_{x^2-y^2}}{}^*\right)^2,$$

and

$$\left(\sigma_{3d_{z^2}}\right)^2(\sigma_{4s})^2(\pi_{3d_{xz}})^2(\pi_{3d_{yz}})^2\left(\delta_{3d_{x^2-y^2}}\right)^2(\delta_{3d_{xy}}{}^*)^2,$$

each of which contributes 5%. We will use Cr_2 as a representative case for this group of four molecules.

To illustrate how KS-DFT models these states, we compare the CASSCF description of Cr_2 to the descriptions given by four of the exchange–correlation functionals studied here, in particular, τ-HCTHhyb, M06-L, PBE0 and MPW1K. The first two functionals are among the best functionals for SP-ECP computed bond energies, and the last two are among the least accurate functionals (which is not surprising in the case of MPW1K since generalized gradient approximation functionals with a percentage of Hartree–Fock exchange as high (42.8%) as that in this functional are not designed for treating multireference systems). For all four of these functionals, we found net α electron density located on Cr-1 and net β electron density located on Cr-2; the spin densities given by the Hirshfeld population on Cr-1 for τ-HCTHhyb, M06-L, PBE0, and MPW1K are, respectively, 3.08, 2.96, 3.69, and 4.06. The spin density on Cr-2 has the same value as on Cr-1 but with a negative sign (which means a net β electron density on Cr-2, and a total

open-shell singlet for the molecule). The electronic configurations given by all of these four functionals may be written as

$$\left(\sigma_{3d_{z2}}\right)^2(\sigma_{4s})^2(\pi_{3d_{xz}})^2(\pi_{3d_{yz}})^2\left(\delta_{3d_{x^2-y^2}}\right)^2(\delta_{3d_{xy}})^2,$$

where we combined the spin–orbitals with similar character together. This illustrates a general aspect of the results, namely that the quantitative inaccuracies need not result from getting the orbital occupancies wrong; just as for single-reference systems, there can be significant errors in the bond energies even for a qualitatively correct description of the orbital occupancies. This may be attributed to the quantitative dependences of the exchange–correlation functionals on spin densities, their gradients, and – for meta functionals – on the kinetic energy densities. In other cases, as illustrated in the next subsection, we do indeed find different orbital occupancies.

5.B.2. VNb and V_2. For VNb, the dominant configuration given by the CASSCF wave function is

$$\left(\sigma_{3d_{z2}-4d_{z2}}\right)^2(\sigma_{4s-5s})^2(\pi_{3d_{xz}-4d_{xz}})^2(\pi_{3d_{yz}-4d_{yz}})^2\left(\delta_{3d_{x^2-y^2}-4d_{x^2-y^2}}\right)^1 \times \left(\delta_{3d_{xy}-4d_{xy}}\right)^1,$$

which contributes 73% to the total wave function. For V_2, the dominant configuration given by the CASSCF wave function is

$$\left(\sigma_{3d_{z2}}\right)^2(\sigma_{4s})^2(\pi_{3d_{xz}})^2(\pi_{3d_{yz}})^2\left(\delta_{3d_{x^2-y^2}}\right)^1(\delta_{3d_{xy}})^1,$$

which contributes 71% to the total wave function.

We investigate the electronic configuration given by KS-DFT for V_2 as an example. The net atomic spin densities given by τ-HCTHhyb, M06-L, and PBE0 are the same, with 1.00 on V-1 and 1.00 on V-2; however, for MPW1K, the spin density on V-1 is 3.62 while on V-2 it is −1.62. The electronic configurations given by τ-HCTHhyb and PBE0 are

$$\left(\sigma_{3d_{z2}}\right)^2(\sigma_{4s})^2(\pi_{3d_{xz}})^2(\pi_{3d_{yz}})^2\left(\tilde{\delta}\right)^1\left(\tilde{\delta}\right)^1,$$

where $\tilde{\delta}$ indicates that the orbital symmetry is significantly broken, and one cannot assign the MO cleanly to either $3d_{x^2-y^2}$ or $3d_{xy}$ AO. For M06-L the electronic configuration for the lowest-energy stabilized solution is

$$\left(\sigma_{3d_{z2}}\right)^2(\sigma_{4s})^2(\pi_{3d_{xz}})^2(\pi_{3d_{yz}})^2\left(\delta_{3d_{x^2-y^2}}\right)^1(\delta_{3d_{xy}})^1;$$

which is qualitatively correct, but for MPW1K, the electronic configuration is

$$\left(\sigma_{3d_{z2}}\right)^1(\sigma_{4s})^2(\pi_{3d_{xz}})^2(\pi_{3d_{yz}})^2\left(\tilde{\delta}\right)^2\left(\tilde{\delta}\right)^1,$$

which is not the dominant electronic configuration given by CASSCF.

5.B.3. Rh_2. The dominant configuration given by the CASSCF wave function is

$$\left(\sigma_{4d_{z2}}\right)^2(\sigma_{5s})^2(\pi_{4d_{xz}})^2(\pi_{4d_{yz}})^2\left(\delta_{4d_{x^2-y^2}}\right)^2(\delta_{4d_{xy}})^2 \times \left(\sigma_{4d_{z2}}{}^*\right)^1(\pi_{4d_{xz}}{}^*)^1(\pi_{4d_{yz}}{}^*)^1\left(\delta_{4d_{x^2-y^2}}{}^*\right)^2(\delta_{4d_{xy}}{}^*)^1$$

which contributes 71% to the total wave function.

The net atomic spin densities for Rh-1 given by τ-HCTHhyb, M06-L, PBE0, and MPW1K are, respectively, 1.93, 2.00, 2.00, and 1.91; while for Rh-2 they are 2.07, 2.00, 2.00 and 2.09. More detailed examination shows that M06-L gives the same electronic configuration as CASSCF, with well-defined orbital characters (*i.e.*, σ, π, or δ characters); while for τ-HCTHhyb, PBE0, and MPW1K, the BS-UKS orbitals are significantly distorted, and one cannot identify the orbital character and the symmetry of the orbital.

5.B.4. VCr and NbCr. For VCr, the dominant configuration in the CASSCF wave function is

$$\left(\sigma_{3d_{z2}}\right)^2(\sigma_{4s})^2(\pi_{3d_{xz}})^2(\pi_{3d_{yz}})^2\left(\delta_{3d_{x^2-y^2}}\right)^2(\delta_{3d_{xy}})^1,$$

which contributes 60% to the total wave function. For NbCr, the dominant configuration given by the CASSCF wave function is

$$\left(\sigma_{3d_{z2}-4d_{z2}}\right)^2(\sigma_{4s-5s})^2(\pi_{3d_{xz}-4d_{xz}})^2(\pi_{3d_{yz}-4d_{yz}})^2\left(\delta_{3d_{x^2-y^2}-4d_{x^2-y^2}}\right)^2 \times \left(\delta_{3d_{xy}-4d_{xy}}\right)^1,$$

which contributes 57% to the total wave function.

Next we compare the above electronic configuration for NbCr (whose experimental bond energy is available) to the electronic configurations of the BS-UKS-DFT calculations. The spin-densities on Nb as given, respectively, by τ-HCTHhyb, M06-L, PBE0, and MPW1K are 1.34, −1.58, 2.04, and 2.63; on Cr the spin densities are −0.34, 2.58, −1.04, and −1.63. Further examination of the electronic configurations shows that those given by τ-HCTHhyb, PBE0, and MPW1K are the same as CASSCF, but for M06-L, the electronic configuration of the lowest-energy stabilized BS solution is

$$\left(\sigma_{3d_{z2}-4d_{z2}}\right)^2(\sigma_{4s-5s})^1(\pi_{3d_{xz}-4d_{xz}})^2(\pi_{3d_{yz}-4d_{yz}})^2\left(\delta_{3d_{x^2-y^2}-4d_{x^2-y^2}}\right)^2 \times \left(\delta_{3d_{xy}-4d_{xy}}\right)^2,$$

which differs from the one given by CASSCF.

5.C. Possible sources of errors

A previous study[9] found that the signed error (SE) for the bond dissociation energy of V_2 is related to the KS orbital energy difference between the $3d_{z^2}$ and 4s orbitals $\left(\Delta\varepsilon = \varepsilon_{3d_{z2}} - \varepsilon_{4s}\right)$, because two key sigma orbitals $\left(\sigma_{3d_{z2}}\right.$ and $\left.\sigma_{4s}\right)$ are hybridized from these two AOs. A larger $\Delta\varepsilon$ tends to give a negative SE, and a smaller $\Delta\varepsilon$ tends to give a positive MSE. The electronic structures of the diatomics studied in the present work are similar to V_2, and the compositions of the MOs are very alike. In the case of V_2, the percentage of nonlocal exchange is also well correlated with the MSE. However, in our present study, a few meta functionals with more than 25% Hartree–Fock exchange, in particular, M05, M06, and MN15 (with Hartree–Fock exchange percentages of, respectively, 28, 27, and 44%), are still able to perform quite well among all the functionals we tested when used with the ECP basis; we attribute this to the

careful parameterization of these functionals, which were designed to be broadly accurate.

In the present study, as in all of our applications of KS-DFT, we are seeking the lowest-energy solution (for a pre-specified M_S quantum number) in the BS-UKS formulation. The resulting solution is our best approximation, for a given exchange–correlation functional, to the ground-state energy, and there is no guarantee that the approximate exchange–correlation functional predicts the correct electronic configuration. Furthermore, we have found that attempting to "correct" the symmetry of the Slater determinant does not necessarily lead to better results.[11] The broken-symmetry character of the solution can make the symmetry assignment of the electronic state ambiguous or invalid, which can be a problem for excited states. But we cannot judge the success of the density functional entirely by comparing the orbitals to those of a wave function calculation (for example, a CASSCF calculation) because the goal of KS-DFT is to predict the ground-state energy and density, not to predict the multi-configurational wave function. In applications to practical problems, an accurate wave function calculation is often unavailable and unaffordable, and the applier of DFT does not necessarily know the symmetry of the correct ground state. The exact density can be found from the exact wave function, which has all the correct symmetries; and the exact density can also be found from the Slater determinant obtained with an exact density functional, but we should keep in mind that the Slater determinant, although it gives the exact density, does not necessarily have the same symmetry properties as the exact wave function. Therefore, we optimize the Slater determinant to minimize the calculated ground-state energy, independent of symmetry considerations except for the total electron spin component M_S; this provides a systematic approach whose accuracy can be tested for small systems, and that is what we have done in the present article.

5.D. Future

It is a continuing challenge to develop more universal Kohn–Sham exchange–correlation functionals[74] that can improve the performance on this kind of problem. In addition, it will be interesting in future work to see how well multi-configuration pair-density functional theory[75] (MC-PDFT) can do on the present test set. MC-PDFT combines density functional theory with multi-configurational reference wave functions. We have already seen improvement for transition metal systems over Kohn–Sham density functional theory by using the MC-PDFT theoretical framework.[76]

6. Summary

Kohn–Sham density functional theory represents the density with a single-configuration (in particular, a single Slater determinant) reference function. In this work, we explore the ability of Kohn–Sham density functional theory, with modern exchange–correlation functionals, to predict the bond lengths and bond dissociation energies of various 3d and 4d bimetallic diatomic molecules. These systems are strongly correlated and present a serious challenge for KS-DFT (as well as for wave function theory); in fact these dimers are expected to be more difficult to treat than, for example, closed-shell organometallics, and hence they provide a critical test relevant to the treatment of open-shell systems that might occur in catalytically active sites and catalytic intermediates. We find that most of the functionals show a mean unsigned error in bond energies larger than 20 kcal mol^{-1}; in fact the median of the 50 mean unsigned errors is 28 kcal mol^{-1} when using ECPs and 26 kcal mol^{-1} when using the DKH method. Furthermore, we find that the median of the 50 mean unsigned errors in bond length is 0.08 Å using effective core potentials and 0.12 Å using the DKH method.

Nevertheless, a few XC functionals, in particular, M06-L, OreLYP, and N12-SX are able to predict both bond energies with a mean unsigned error of less than 10 kcal mol^{-1}, and bond lengths with a mean unsigned error of less than 0.07 Å. A final choice of application for a complex application will often have to also consider bond energies, barrier heights, and weak interactions for main-group molecules, which are sometimes critical in catalytic cycles, and we refer the reader to other studies[3,77–83,95,102,117,122] for comparisons of functionals in a broader context.

For transition-metal systems in which metal–metal bond making or bond breaking is involved, even if one is using the functionals with best average performance, the results may have significant errors; and predicted differences smaller than 10 kcal mol^{-1} between different reaction paths should be used with caution. As demonstrated in this work, bimetallic diatomics are clearly a challenge for single-reference-based Kohn–Sham density functional theory, and the results are less accurate than those obtained for the main-group chemistry or for transition-metal bonds to nonmetallic ligands.

Acknowledgements

The authors are grateful to Steven Mielke for assistance with some of the calculations. This work was supported in part by the U.S. Department of Energy, Office of Basic Energy Sciences, Division of Chemical Sciences, under award DE-SC0012702 to the Inorganometallic Catalyst Design Center.

References

1 J. P. McInnis, M. Delferro and T. J. Marks, *Acc. Chem. Res.*, 2014, **47**, 2545.
2 D. C. Powers and T. Ritter, *Acc. Chem. Res.*, 2012, **45**, 840.
3 W. Kohn and L. J. Sham, *Phys. Rev.*, 1965, **140**, A1133.
4 R. Peverati and D. G. Truhlar, *Philos. Trans. R. Soc., A*, 2014, **372**, 20120476.
5 G. L. Gutsev and C. W. Bauschlicher, *J. Phys. Chem. A*, 2003, **107**, 4755.
6 N. E. Schultz, Y. Zhao and D. G. Truhlar, *J. Phys. Chem. A*, 2005, **109**, 4388.
7 F. Furche and J. P. Perdew, *J. Chem. Phys.*, 2006, **124**, 044103.

8 G. L. Gutsev, C. A. Weatherford, P. Jena, E. Johnson and B. R. Ramachandran, *J. Phys. Chem. A*, 2012, **116**, 10218.
9 W. Zhang, D. G. Truhlar and M. Tang, *J. Chem. Theory Comput.*, 2014, **10**, 2399.
10 Y.-L. Wang, H.-S. Hu, W.-L. Li, F. Wei and J. Li, *J. Am. Chem. Soc.*, 2016, **138**, 1126.
11 S. Luo, B. Averkiev, K. R. Yang, X. Xu and D. G. Truhlar, *J. Chem. Theory Comput.*, 2014, **10**, 102.
12 S. Luo and D. G. J. Truhlar, *J. Chem. Theory Comput.*, 2012, **8**, 4112.
13 J. Čížek, *J. Chem. Phys.*, 1966, **45**, 4256.
14 J. A. Pople, R. Krishnan, H. B. Schlegel and J. S. Binkley, *Int. J. Quantum Chem.*, 1978, **14**, 545.
15 R. J. Bartlett and G. D. Purvis, *Int. J. Quantum Chem.*, 1978, **14**, 561.
16 G. E. Scuseria, C. L. Janssen and H. F. Schaefer, *J. Chem. Phys.*, 1988, **89**, 7382.
17 K. Raghavachari, G. W. Trucks, J. A. Pople and M. Head-Gordon, *Chem. Phys.*, 1989, **157**, 479.
18 For recent work, see for instances: (*a*) L. Hu and H. Chen, *J. Chem. Theory Comput.*, 2015, **11**, 4601; (*b*) Y. Sun and H. Chen, *J. Chem. Theory Comput.*, 2014, **10**, 579; (*c*) Y. Sun and H. Chen, *J. Chem. Theory Comput.*, 2013, **9**, 4735; (*d*) J. L. Bao, H. S. Yu, K. Duanmu, M. A. Makeev, X. Xu and D. G. Truhlar, *ACS Catal.*, 2015, **5**, 2070. For a review, see C. J. Cramer and D. G. Truhlar, *Phys. Chem. Chem. Phys.*, 2009, **11**, 10757.
19 X. Xu, W. Zhang, M. Tang and D. G. Truhlar, *J. Chem. Theory Comput.*, 2015, **11**, 2036.
20 (*a*) J. L. Bao, A. Sand, L. Gagliardi and D. G. Truhlar, *J. Chem. Theory Comput.*, 2016, **12**, 4274; (*b*) J. L. Bao, S. O. Odoh, L. Gagliardi and D. G. Truhlar, *J. Chem. Theory Comput.*, 2017, DOI: 10.1021/acs.jctc.6b01102.
21 D. Porezag, M. R. Pederson and A. Y. Liu, *Phys. Rev. B: Condens. Matter Mater. Phys.*, 1999, **60**, 14132.
22 C. van Wüllen, *Int. J. Quantum Chem.*, 1996, **58**, 147.
23 Y.-K. Han and K. Hirao, *Chem. Phys. Lett.*, 2000, **324**, 453.
24 Y. Yang, M. N. Weaver and K. M. Merz, Jr., *J. Phys. Chem. A*, 2009, **113**, 9843.
25 X. Xu and D. G. Truhlar, *J. Chem. Theory Comput.*, 2011, **7**, 2766.
26 X. Xu and D. G. Truhlar, *J. Chem. Theory Comput.*, 2012, **8**, 80.
27 S. M. Casey and D. G. Leopold, *J. Phys. Chem.*, 1993, **97**, 816.
28 B. Simard, M.-A. Lebeault-Dorget, A. Marijnissen and J. J. ter Meulen, *J. Chem. Phys.*, 1998, **108**, 9668.
29 V. E. Bondybey and J. H. English, *Chem. Phys. Lett.*, 1983, **94**, 443.
30 E. M. Spain, J. M. Behm and M. D. Morse, *J. Chem. Phys.*, 1992, **96**, 2511.
31 C. Cossé, M. Fouassier, T. Mejean, M. Tranquille, D. P. DiLella and M. Moskovits, *J. Chem. Phys.*, 1980, **73**, 6076.
32 J. B. Hopkins, P. R. R. Langridge-Smith, M. D. Morse and R. E. Smalley, *J. Chem. Phys.*, 1983, **78**, 1627.
33 J. D. Langenberg and M. D. Morse, *J. Chem. Phys.*, 1998, **108**, 2331.
34 S. M. Sickafoose, J. D. Langenberg and M. D. Morse, *J. Phys. Chem. A*, 2000, **104**, 3521.
35 A. M. James, P. Kowalczyk, E. Langlois, M. D. Campbell, A. Ogawa and B. Simard, *J. Chem. Phys.*, 1994, **101**, 4485.
36 A. M. James, P. Kowalczyk and B. Simard, *Chem. Phys. Lett.*, 1993, **216**, 512.
37 R. Nagarajan and M. D. Morse, *J. Chem. Phys.*, 2007, **127**, 074304.
38 C. A. Arrington, T. Blume, M. D. Morse, M. Doverstål and U. Sassenberg, *J. Phys. Chem.*, 1994, **98**, 1398.
39 R. Seeger and J. A. Pople, *J. Chem. Phys.*, 1977, **66**, 3045.
40 R. Bauernschmitt and R. Ahlrichs, *J. Chem. Phys.*, 1996, **104**, 9047.
41 I. M. Alecu, J. Zheng, Y. Zhao and D. G. Truhlar, *J. Chem. Theory Comput.*, 2010, **6**, 2872.
42 N. B. Balabanov and K. A. Peterson, *J. Chem. Phys.*, 2005, **123**, 064107.
43 (*a*) M. Douglas and N. M. Kroll, *Ann. Phys.*, 1974, **82**, 89; (*b*) G. Jansen and B. A. Hess, *Phys. Rev. A: At., Mol., Opt. Phys.*, 1989, **39**, 6016.
44 C. L. Pekeris, *Phys. Rev.*, 1934, **45**, 98.
45 I. N. Levine, *Molecular Spectroscopy*, John Wiley & Sons, Inc., Chichester, 1975.
46 J. Sansonetti, W. Martin and S. Young, *Handbook of Basic Atomic Spectroscopic Data*, Version 1.00, National Institute of Standards and Technology, Gaithersburg, MD, 2003, available at http://physics.nist.gov/Handbook, accessed Aug. 10, 2016.
47 S. R. Langhoff and C. W. Kern, in *Modern Theoretical Chemistry*, ed. H. F. Schaefer III, Plenum Press, New York, 1977, vol. 3, p. 381.
48 H. A. Bethe and E. E. Salpeter, *Quantum Mechanics of One- and Two-Electron Atoms*, Springer-Verlag, Berlin, 1957.
49 H.-J. Werner and P. J. Knowles, *J. Chem. Phys.*, 1985, **82**, 5053.
50 P. J. Knowles and H.-J. Werner, *Chem. Phys. Lett.*, 1985, **115**, 259.
51 A. Berning, M. Schweizer, H.-J. Werner, P. J. Knowles and P. Palmieri, *Mol. Phys.*, 2000, **98**, 1823.
52 F. Weigend and R. Ahlrichs, *Phys. Chem. Chem. Phys.*, 2005, **7**, 3297.
53 C. T. Campos and F. E. Jorge, *Mol. Phys.*, 2013, **111**, 167.
54 K. A. Peterson, D. Figgen, M. Dolg and H. Stoll, *J. Chem. Phys.*, 2007, **126**, 124101.
55 B. Metz, M. Schweizer, H. Stoll, M. Dolg and W. Liu, *Theor. Chim. Acta*, 2000, **104**, 22.
56 H.-J. Werner, P. J. Knowles, G. Knizia, F. R. Manby and M. Schütz, *et al.*, *Molpro*, version 2015.1; see http://www.molpro.net.
57 T. J. Lee and P. R. Taylor, *Int. J. Quantum Chem.*, 1989, **36**, 199.
58 O. Tishchenko, J. Zheng and D. G. Truhlar, *J. Chem. Theory Comput.*, 2008, **4**, 1208.
59 R. Seeger and J. A. Pople, *J. Chem. Phys.*, 1976, **66**, 3045.

60 H. B. Schlegel and J. J. W. McDouall, in *Computational Advances in Organic Chemistry: Molecular Structure Reactivity*, ed. C. Ögritir and G. Csizmadia, Kluwer, Dordrecht, 1991, NATO ASI Series, vol. 330, p. 167.
61 R. Bauernschmitt and R. Ahlrichs, *J. Chem. Phys.*, 1996, **104**, 9047.
62 N. Schuch and F. Verstraete, *Nat. Phys.*, 2009, **5**, 732.
63 A. Görling, *Phys. Rev. A: At., Mol., Opt. Phys.*, 1993, **47**, 2783.
64 C. R. Jacob and M. Reiher, *Int. J. Quantum Chem.*, 2012, **112**, 3661.
65 F. Weigenda and R. Ahlrichs, *Phys. Chem. Chem. Phys.*, 2005, **7**, 3297.
66 (*a*) D. Andrae, U. Haeussermann, M. Dolg, H. Stoll and H. Preuss, *Theor. Chim. Acta*, 1990, **77**, 123; (*b*) M. Dolg, U. Wedig, H. Stoll and H. Preuss, *J. Chem. Phys.*, 1987, **86**, 866.
67 M. J. Frisch, G. W. Trucks, H. B. Schlegel, G. S. Scuseria, M. A. Robb and J. R. Cheeseman, *et al.*, *Gaussian 09 (revision D.01)*, Gaussian, Inc., Wallingford CT, 2009.
68 F. Aquilante, J. Autschbach, R. K. Carlson, L. F. Chibotaru, M. G. Delcey and L. De Vico, *et al.*, *J. Comput. Chem.*, 2016, **37**, 506.
69 X. Xu and D. G. Truhlar, *J. Chem. Theory Comput.*, 2012, **8**, 80.
70 K. Andersson, *Theor. Chem. Acc.*, 2003, **110**, 218.
71 J. Sun, B. Xiao, Y. Fang, R. Haunschild, P. Hao, A. Ruzsinszky, G. I. Csonka, G. E. Scuseria and J. P. Perdew, *Phys. Rev. Lett.*, 2013, **111**, 106401.
72 A. D. Becke and K. E. Edgecombe, *J. Chem. Phys.*, 1990, **92**, 5397.
73 B. Silvi and A. Savin, *Nature*, 1994, **371**, 683.
74 H. S. Yu, S. L. Li and D. G. Truhlar, *J. Chem. Phys.*, 2016, **145**, 130901.
75 L. Gagliardi, D. G. Truhlar, G. Li Manni, R. K. Carlson, C. E. Hoyer and J. L. Bao, *Acc. Chem. Res.*, 2017, **50**, 66.
76 J. L. Bao, S. O. Odoh, L. Gagliardi and D. G. Truhlar, *J. Chem. Theory Comput.*, 2017, DOI: 10.1021/acs.jctc.6b01102.
77 K. Remya and C. H. Suresh, *J. Comput. Chem.*, 2011, **34**, 1341.
78 L. Goerigk and S. Grimme, *Phys. Chem. Chem. Phys.*, 2011, **13**, 6670.
79 O. N. Faza, R. Á. Rodríguez and C. S. López, *Theor. Chem. Acc.*, 2011, **128**, 647.
80 S. Zahn, D. R. Macfarlane and E. I. Izgorodina, *Phys. Chem. Chem. Phys.*, 2013, **15**, 13664.
81 T. Anacker and J. Friedrich, *J. Comput. Chem.*, 2014, **35**, 634.
82 S. Rayne and K. Forest, *Can. J. Chem.*, 2016, **94**, 251.
83 S. Rayne and K. Forest, *Comput. Theor. Chem.*, 2016, **1090**, 147.
84 J. P. Perdew, A. Ruzsinsky, G. I. Csonka, O. A. Vydrov, G. E. Scuseria, L. A. Constantin, X. Zhou and K. Burke, *Phys. Rev. Lett.*, 2008, **100**, 136406.
85 Y. Zhao and D. G. Truhlar, *J. Chem. Phys.*, 2008, **128**, 184109.
86 R. Peverati, Y. Zhao and D. G. Truhlar, *J. Phys. Chem. Lett.*, 2011, **2**, 1911.
87 A. D. Becke, *Phys. Rev. A: At., Mol., Opt. Phys.*, 1988, **38**, 3098.
88 C. Lee, W. Yang and R. G. Parr, *Phys. Rev. B: Condens. Matter Mater. Phys.*, 1988, **37**, 785.
89 N. E. Schultz, Y. Zhao and D. G. Truhlar, *J. Phys. Chem. A*, 2005, **109**, 11127.
90 N. C. Handy and A. J. Cohen, *Mol. Phys.*, 2001, **99**, 403.
91 A. J. Thakkar and S. P. McCarthy, *J. Chem. Phys.*, 2009, **131**, 134109.
92 J. P. Perdew, K. Burke and M. Ernzerhof, *Phys. Rev. Lett.*, 1996, **77**, 3865.
93 Y. Zhang and W. Yang, *Phys. Rev. Lett.*, 1998, **80**, 890.
94 B. Hammer, L. B. Hansen and J. K. Norskov, *Phys. Rev. B: Condens. Matter Mater. Phys.*, 1999, **59**, 7413.
95 H. S. Yu, W. Zhang, P. Verma, X. He and D. G. Truhlar, *Phys. Chem. Chem. Phys.*, 2015, **17**, 12146.
96 R. Peverati and D. G. Truhlar, *J. Chem. Theory Comput.*, 2012, **8**, 2310.
97 Y. Zhao and D. G. Truhlar, *J. Chem. Phys.*, 2006, **125**, 194101.
98 R. Peverati and D. G. Truhlar, *J. Phys. Chem. Lett.*, 2011, **2**, 2810.
99 J. Sun, R. Haunschild, B. Xiao, I. W. Bulik, G. E. Scuseria and J. P. Perdew, *J. Chem. Phys.*, 2013, **138**, 044113.
100 A. D. Boese and N. C. Handy, *J. Chem. Phys.*, 2002, **116**, 9559.
101 R. Peverati and D. G. Truhlar, *Phys. Chem. Chem. Phys.*, 2012, **14**, 13171.
102 H. S. Yu, X. He and D. G. Truhlar, *J. Chem. Theory Comput.*, 2016, **12**, 1280.
103 C. Adamo and V. Barone, *Chem. Phys. Lett.*, 1997, **274**, 242.
104 P. J. Stephens, C. F. Chabalowski and M. J. Frisch, *J. Phys. Chem.*, 1994, **98**, 11623.
105 F. A. Hamprecht, A. Cohen, D. J. Tozer and N. C. Handy, *J. Chem. Phys.*, 1998, **109**, 6264.
106 T. W. Keal and D. J. Tozer, *J. Chem. Phys.*, 2005, **123**, 121103.
107 Y. Zhao and D. G. Truhlar, *J. Phys. Chem. A*, 2004, **108**, 6908.
108 B. J. Lynch, P. L. Fast, M. Harris and D. G. Truhlar, *J. Phys. Chem. A*, 2000, **104**, 4811.
109 Y. Zhao and D. G. Truhlar, *J. Phys. Chem. A*, 2004, **108**, 6908.
110 M. W. Hoe, A. J. Cohen and N. C. Handy, *Chem. Phys. Lett.*, 2001, **341**, 319.
111 C. Adamo and V. Barone, *J. Chem. Phys.*, 1999, **110**, 6158.
112 R. Peverati and D. G. Truhlar, *J. Chem. Phys.*, 2011, **135**, 191102.
113 J. B. Krieger, J. Chen, G. J. Iafrate and A. Savin, in *Electron Correlations and Materials Properties*, ed. A. Gonis and N. Kioussis, Plenum, New York, 1999, p. 463.
114 Y. Zhao and D. G. Truhlar, *Acc. Chem. Res.*, 2008, **41**, 157.
115 Y. Zhao and D. G. Truhlar, *J. Chem. Theory Comput.*, 2008, **4**, 1849.
116 Y. Zhao, B. J. Lynch and D. G. Truhlar, *Phys. Chem. Chem. Phys.*, 2005, **7**, 43.

117 Y. Zhao and D. G. Truhlar, *Theor. Chem. Acc.*, 2008, **120**, 215.
118 Y. Zhao and D. G. Truhlar, *J. Phys. Chem. A*, 2006, **110**, 13126.
119 Y. Zhao and D. G. Truhlar, *J. Phys. Chem. A*, 2005, **109**, 5656.
120 V. N. Staroverov, G. E. Scuseria, J. Tao and J. P. Perdew, *J. Chem. Phys.*, 2003, **119**, 12129.
121 A. D. Boese and N. C. Handy, *J. Chem. Phys.*, 2002, **116**, 9559.
122 H. S. Yu, X. He, S. L. Li and D. G. Truhlar, *Chem. Sci.*, 2016, **7**, 5032.
123 J. Heyd, G. E. Scuseria and M. Ernzerhof, *J. Chem. Phys.*, 2003, **118**, 8207.
124 T. M. Henderson, A. F. Izmaylov, S. Scalmani and G. E. Scuseria, *J. Chem. Phys.*, 2009, **131**, 044108.
125 J. Chai and M. Head-Gordon, *J. Chem. Phys.*, 2008, **128**, 084106.
126 J. Chai and M. Head-Gordon, *Phys. Chem. Chem. Phys.*, 2008, **10**, 6615.
127 R. Peverati and D. G. Truhlar, *J. Phys. Chem. Lett.*, 2011, **2**, 2810.
128 R. Peverati and D. G. Truhlar, *Phys. Chem. Chem. Phys.*, 2012, **14**, 16187.

